JVST A
Journal of Vacuum Science & Technology A
ARTICLE
avs.scitation.org/journal/jva

# Heteroepitaxial growth of β-$Ga_2O_3$ films on SiC via molecular beam epitaxy

Cite as: J. Vac. Sci. Technol. A **38**, 063406 (2020); doi: 10.1116/6.0000452
Submitted: 10 July 2020 · Accepted: 28 September 2020 ·
Published Online: 15 October 2020

Neeraj Nepal,[1,a)] D. Scott Katzer,[1] Brian P. Downey,[1] Virginia D. Wheeler,[1] Luke O. Nyakiti,[2] David F. Storm,[1] Matthew T. Hardy,[1] Jaime A. Freitas,[1] Eric N. Jin,[1,b)] Diego Vaca,[3] Luke Yates,[3] Samuel Graham,[3] Satish Kumar,[3] and David J. Meyer[1]

## AFFILIATIONS

[1]Electronics Science and Technology Division, U. S. Naval Research Laboratory, 4555 Overlook Ave SW, Washington, DC 20375
[2]Department of Materials Science and Engineering, Texas A&M University, College Station, Texas 77843
[3]George W. Woodruff School of Mechanical Engineering, Georgia Institute of Technology, Atlanta, Georgia 30332

**Note:** This paper is part of the Special Topic Collection on Gallium Oxide Materials and Devices.
[a)]**Electronic mail:** neeraj.nepal@nrl.navy.mil
[b)]National Academy of Sciences National Research Council Postdoctoral Fellow

## ABSTRACT

β-$Ga_2O_3$ is a promising ultrawide bandgap semiconductor for next generation radio frequency electronics. However, its low thermal conductivity and inherent thermal resistance provide additional challenges in managing the thermal response of β-$Ga_2O_3$ electronics, limiting its power performance. In this paper, we report the heteroepitaxial growth of β-$Ga_2O_3$ films on high thermal conductivity 4H-SiC substrates by molecular beam epitaxy (MBE) at 650 °C. Optimized MBE growth conditions were first determined on sapphire substrates and then used to grow β-$Ga_2O_3$ on 4H-SiC. X-ray diffraction measurements showed single phase ($\bar{2}01$) β-$Ga_2O_3$ on (0001) SiC substrates, which was also confirmed by TEM measurements. These thin films are electrically insulating with a ($\bar{4}02$) peak rocking curve full-width-at-half-maximum of 694 arc sec and root mean square surface roughness of ∼2.5 nm. Broad emission bands observed in the luminescence spectra, acquired in the spectral region between near infrared and deep ultraviolet, have been attributed to donor-acceptor pair transitions possibly related to Ga vacancies and its complex with O vacancies. The thermal conductivity of an 81 nm thick $Ga_2O_3$ layer on 4H-SiC was determined to be $3.1 \pm 0.5$ W/m K, while the measured thermal boundary conductance (TBC) of the $Ga_2O_3$/SiC interface is $140 \pm 60$ MW/$m^2$ K. This high TBC value enables the integration of thin β-$Ga_2O_3$ layers with high thermal conductivity substrates to meliorate thermal dissipation and improve device thermal management.

https://doi.org/10.1116/6.0000452

## I. INTRODUCTION

After more than two decades of research, wide bandgap semiconductors such as GaN and SiC have been readily adapted for high power/frequency applications due to their robustness, ability to switch at higher frequencies, and higher power density capability.[1,2] Significant investments in basic materials and module-level application research have resulted in high performing devices that are rapidly approaching their physical limitations.[3] To continue advancements in high power/frequency devices, there is a need to look beyond GaN and SiC at ultrawide bandgap (UWBG) semiconductors such as $Ga_2O_3$, diamond, high Al content AlGaN, AlN, and cubic BN, which are the next logical candidates because of their wider bandgap and high saturated carrier velocity.[4] Each of these candidates has benefits and limitations for direct incorporation in next generation devices. For instance, previous efforts in III-N materials can be leveraged to realize high-Al containing AlGaN. To attain an AlGaN bandgap of about 4.9 eV, similar to β-$Ga_2O_3$, requires approximately 65% Al mole fraction.[5,6] However, at these levels, the material suffers from low thermal conductivity ($Al_{0.65}Ga_{0.35}N$ is ≤25 W/m K).[7] Additionally, donor and acceptor levels are deeper in AlN and in AlGaN as Al content increases compared to GaN and that makes device level doping and contacts more difficult. In ternary AlGaN alloys, lower carrier mobilities and channel conductivity may be expected as a consequence of increased alloy scattering.[4] Diamond has a bandgap of 5.5 eV and can be p-type doped, but single crystal substrates are expensive, as

well as limited in size and availability. Cubic BN (c-BN) has a wider bandgap, higher thermal conductivity, and has the advantage of possible shallow n- and p-doping levels. However, c-BN has no native substrate and is a metastable phase, which makes it harder to deposit as a single phase high quality film.

$Ga_2O_3$ is an attractive candidate material for high power/frequency devices as it has ultrawide bandgap (4.9 eV), shallow donor level, and inexpensive native substrate.[8] It has several different crystalline phases, and the most stable is β-$Ga_2O_3$, which has a bandgap of 4.5–4.9 eV.[4,8–10] The β phase has a monoclinic lattice (C2/m space group) with lattice parameters of a = 1.223 nm, b = 0.304 nm, c = 0.580 nm, and crystal angle, β = 103.7°. Because of its wide bandgap, it has a large electric field breakdown strength that results in high figures of merit for power and RF devices.[4,8] However, it presents a challenge for power devices due to its low thermal conductivity.[11] Low thermal conductivity may limit its device performance due to thermally accelerated degradation during device operation at high powers.

To take full advantage of the UWBG benefits of higher power handling and power density, thermal management is critical. However, thermal management has also been an issue for a range of other semiconductor technologies including GaAs, Si, and GaN, all of which have found successful use in commercial applications.[12] Many of the techniques or methods used to address this problem in GaN could potentially be employed in $Ga_2O_3$ to accelerate the performance improvements of $Ga_2O_3$ transistors. One approach is to put high thermal conductivity materials in close proximity of the active regions to improve heat removal by spreading heat. In such a case, the thermal boundary conduction through the material interfaces is critical for the overall effectiveness of the thermal management strategy. The main epitaxial quality and interface power dissipation issue is the need to find technologies that help to reduce the local power densities in devices and/or reduce the thermal resistance between the heat generation region and device thermal sink. However, the heterogeneous integration of high thermal conductivity substrates with active semiconductor layers is not trivial since this introduces a thermal boundary resistant between the two layers that can play a significant role in limiting device thermal management performance.

One strategy to improve the performance of $Ga_2O_3$ based devices is through heterostructure design using a thin, epitaxial, conducting $Ga_2O_3$ channel on higher thermal conductivity substrates such as Si, SiC, and diamond. Recent thermal simulations of a β-$Ga_2O_3$ field effect transistor on 4H-SiC have shown a reduction in self-heating that allows the device to be driven at higher gate voltages, allow an 18% increase in peak drain current and 41% reduction in lattice temperature with a corresponding overall performance increase.[13] The monoclinic (010) plane has lattice mismatches of about 20.8, 14.8, and 1.3% with Si(111), diamond, and SiC, respectively. The large lattice mismatch with Si and diamond causes challenges in the direct integration with $Ga_2O_3$. Due to smaller lattice mismatch compared to Si and diamond, the growth of $Ga_2O_3$ on SiC should result in lower density of threading dislocations resulting in higher device performance. However, the challenge of direct integration with any of these substrates is the impact of the thermal boundary conductance which may ultimately limit the overall thermal management.

A recent modeling study on the cooling of $Ga_2O_3$ MESFETs on high thermal conductivity substrates shows that a thermal boundary conductance (TBC) above 120 $MW/m^2$ K keeps the interface from being a limiting factor in device thermal management when films are equal to or less than 1 $\mu$m in thickness.[14] Recent measurements of thermal transport across the interface of exfoliated $Ga_2O_3$ that was transferred to single crystal diamond with van der Waals bonds showed a TBC of 17 $MW/m^2$ K, well within the range of being a limiting factor.[15] The TBC in this case is likely limited by the physics of phonon transport across van der Waals bonds and limitations in contact area. In another study, the growth of $Ga_2O_3$ onto diamond using atomic layer deposition showed that a much higher TBC could be achieved, being on the order of 170 $MW/m^2$ K. However, the use of the amorphous or nanocrystalline ALD grown $Ga_2O_3$ is not sufficient for device's operation.[16] This result does suggest that the direct integration of $Ga_2O_3$ on a high thermal conductivity substrate through epitaxial growth could result in device quality layers with a much higher TBC and lead to an acceptable level of heat transfer across the interface.

There have been only a few previous experimental reports on β-$Ga_2O_3$ growth and devices on SiC substrates.[13,17–19] Field-effect hydrogen gas sensor devices were fabricated using $Ga_2O_3$ layers on a (001) c-plane 6H-SiC substrate prepared by the evaporation of gallium in an oxygen plasma environment at 800 °C.[17] Additionally, chloride vapor phase epitaxy was used to grow textured β-$Ga_2O_3$ layers on Si(111) wafers using a ∼100 nm thick SiC buffer layer.[18] Structural and mechanical properties of hybrid vapor phase epitaxy grown β-$Ga_2O_3$ films on SiC/Si substrates were studied using the nanoindentation method in the film.[19] Although there have been a few different reports of $Ga_2O_3$ synthesis on SiC, epitaxial growth of β-$Ga_2O_3$ on 4H-SiC by molecular beam epitaxy (MBE) and the resulting thermal transport properties have not been reported yet. In this paper, we report heteroepitaxial growth and extensive characterization of β-$Ga_2O_3$ films grown by MBE on 4H-SiC.

## II. EXPERIMENT

β-$Ga_2O_3$ films were grown using MBE to thicknesses between 100 and 200 nm at 650 °C, as measured by thermocouple. Relative Ga flux, and oxygen plasma flow were varied to find optimized β-$Ga_2O_3$ growth parameters on 2-in. diameter c-plane sapphire substrates. Optimized growth parameters consist of a temperature, Ga-flux, and oxygen flow at 300 W RF plasma power of 650 °C, $3 \times 10^{-8}$ Torr, 0.66 SCCM, respectively. These parameters were used for the growth of β-$Ga_2O_3$ on sapphire and Si-face 4H-SiC substrates. As received 2 in. diameter Si-face 4H-SiC substrates were loaded into the preparation chamber under vacuum of $\sim 10^{-9}$–$10^{-10}$ Torr. The substrate was outgassed in a degas heater stage for 30 min at 700 °C and then transferred into the growth chamber at a background pressure of $\sim 10^{-10}$ Torr. It was further heat cleaned at 825 °C for 10 min in the growth chamber and then the substrate temperature was reduced to 650 °C for β-$Ga_2O_3$ growth. Ga and $O_2$ plasma source shutters were opened together to start the growth and the growth was monitored *in situ* by reflection high-energy electron diffraction. Figure 1(a) shows a layer structure schematic of the MBE grown films. The β-$Ga_2O_3$ films were

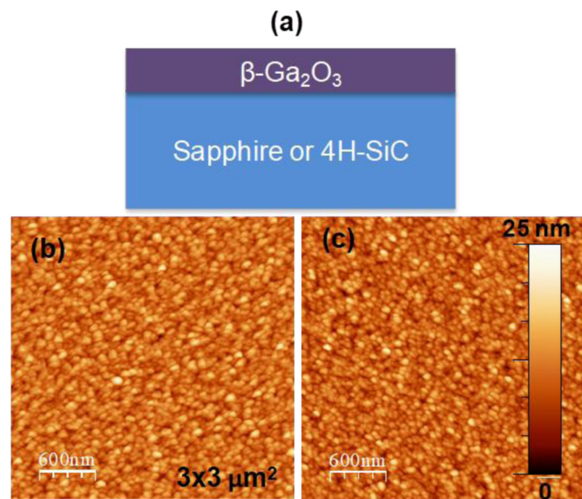


**FIG. 1.** (a) Schematic of the layer structure β-$Ga_2O_3$ on sapphire and 4H-SiC. Surface morphology of β-$Ga_2O_3$ on (b) sapphire and (c) 4H-SiC.

directly grown on SiC without any buffer or intentional interfacial layer and characterized using morphological, structural, electrical, optical, and thermal techniques.

The surface morphology all films were characterized using Bruker Dimension FastScan atomic force microscopy (AFM) in the tapping mode. High resolution x-ray diffraction (HRXRD) system of 9 kW from Rigaku, that employs a rotating Cu anode to produce Cu-$K_\alpha$ radiation, was used to verify the crystalline quality of the β-$Ga_2O_3$ films using θ–2θ diffraction and RC measurements. Film thicknesses and surface roughness were measured using x-ray reflectivity (XRR) measurements at the G2 beamline of the Cornell High Energy Synchrotron Source. The crystal structure of these β-$Ga_2O_3$ layers and interfaces on 4H-SiC and on c-plane sapphire were characterized using a FEI Titan aberration-corrected, monochromated, environmental transmission electron microscopy (TEM). TEM sample's lamella were fabricated on an FEI Strata Dual Beam FIB/SEM System. Prior to FIB milling, the samples were capped with Au and Pt beam-ionization protective layers. High resolution phase contrast and selected area electron diffraction (SAED) imaging techniques were obtained using FEI Tecnai G2 F-20 ST FE-TEM operated at 200 kV. Post imaging analysis involved the use of fast Fourier transform (FFT) and inverse fast Fourier transform to index the reflecting planes and assist in crystallographic orientation relationship determination. All as-deposited films are insulating as measured by contactless resistivity measurements using a Lehighton Electronics Inc. 1510B system. The bandgap of the films was measured using a Filmetrics F10-RT-UV reflection and transmission measurement system. The Filmetrics setup uses an Energetiq EQ-99x compact high brightness broadband light source. The emission bands from the film were probed by cathodoluminescence (CL) measurements carried out at room temperature and at 5 K. The luminescence excited with an electron beam accelerating voltage of 3 kV was analyzed with a compact fiber optical spectrometer with an integration time of 10 s.

The thermal conductivity of these β-$Ga_2O_3$ layers on 4H-SiC and on c-plane sapphire was characterized using time-domain thermoreflectance (TDTR) measurements. The TDTR measurement setup for this study has been described in Ref. 24. The system consists of a Ti:sapphire ($\lambda = 800$ nm, 40 nJ/pulse) oscillator with ∼150 fs pulse width and a repetition rate of ∼80 MHz. To estimate the thermal conductivity of each type of substrates, TDR measurements were carried out after a 98 nm thick Al layer was deposited on bulk sapphire and bulk 4H-SiC. All Al layers were deposited by e-beam evaporation and their thicknesses were estimated by picosecond acoustics.

## III. RESULTS AND DISCUSSION

MBE growth parameters of β-$Ga_2O_3$ were optimized on 2-in. diameter c-plane sapphire substrates and then transferred to the SiC substrate. The surface morphology of β-$Ga_2O_3$ on 4H-SiC and on c-sapphire are compared in Figs. 1(b) and 1(c). Both films are similar and consist of small island-like structures. The root mean square (RMS) surface roughness of β-$Ga_2O_3$/sapphire and β-$Ga_2O_3$/4H-SiC for $3 \times 3\,\mu m^2$ scan are approximately 2.43 and 2.51 nm, respectively.

XRR thickness measurements on these two samples are presented in Fig. 2. The XRR measurements were carried out at the G2 beamline of the Cornell High Energy Synchrotron Source, where the beam energy was tuned to 10.2 keV. XRR data were fitted using Rigaku GLOBALFIT software. The inset of Fig. 2 shows an example of the fitting of the β-$Ga_2O_3$ on 4H-SiC. XRR measured thicknesses of 124.8 ± 0.5 and 84.8 ± 0.4 nm on sapphire and SiC, respectively, which were similar to the 119 ± 3 and 81 ± 1 nm thicknesses measured by TEM (Fig. 5). XRR measured surface roughness are 2.5 and 2.6 nm on sapphire and SiC, which are consistent with atomic force microscopy (AFM) measured RMS roughness. The difference between XRR and TEM thicknesses may be due to thickness nonuniformity of the film.

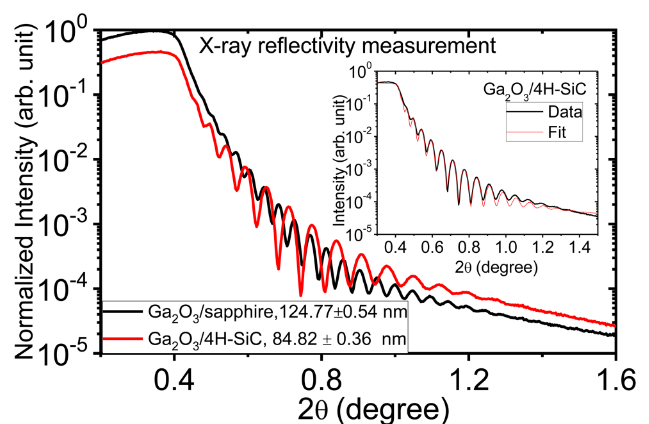


**FIG. 2.** X-ray reflectivity measurement of β-$Ga_2O_3$ on sapphire and 4H-SiC using a 10.2 keV synchrotron light source. Measured thicknesses are approximately 124.77 ± 0.54 and 84.83 ± 0.36 nm, respectively.

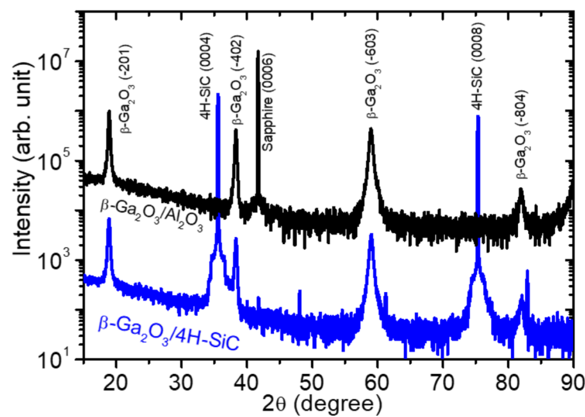


**FIG. 3.** Symmetric θ–2θ XRD curves of β-$Ga_2O_3$ on sapphire (black) and 4H-SiC (blue). First, second, third, and fourth order peaks of (−201) β-$Ga_2O_3$ are clearly measured in the 2θ scan of 10–90°.

Figure 3 shows representative out-of-plane XRD measurements on β-$Ga_2O_3$/sapphire (black line) and β-$Ga_2O_3$/4H-SiC (blue line) between 2θ scan ranges of 10 and 90°. Both measurements show only first-, second-, third-, and fourth-order order peaks ($\bar{2}01$), ($\bar{4}02$), ($\bar{6}03$), and ($\bar{8}04$) from β-$Ga_2O_3$. The shape and position of these peaks shows that the MBE grown β-$Ga_2O_3$ films on both sapphire and 4H-SiC are epitaxial in nature and they have an epitaxial relation of ($\bar{2}01$) β-$Ga_2O_3$||(0001)SiC or sapphire.

Rocking curves (RC) of the ($\bar{4}02$) β-$Ga_2O_3$ peaks for films on sapphire and 4H-SiC are shown in Figs. 4(a) and 4(b) with the RC full-width at the half maximum (FWHM) of 256 and 694 arc sec, respectively. Since the deposition of β-$Ga_2O_3$ film was optimized on sapphire, it has narrower FWHM showing higher quality compared to that on 4H-SiC. There may be some increasing of the FWHM due to the smaller thickness of the film on SiC, as RC FWHM decreases with increasing film thickness. SiC has lower lattice constant mismatch with $Ga_2O_3$ (1.3%) compared to sapphire (6.6%), which should result in better crystalline quality films; however, it is difficult to ensure $Ga_2O_3$ nucleation without unintentional $SiO_x$ formation. Forming an abrupt, amorphous interface-oxide-free interface is also important for minimizing the interfacial thermal boundary resistance.

To further investigate the crystal structure of β-$Ga_2O_3$ films and interface with substrate, two cross-sectional TEM sample lamella were fabricated from each of the substrate using an *in situ* focused ion beam (FIB) lift out technique. Figures 5(a) and 5(b) show high resolution phase contrast micrographs of the β-$Ga_2O_3$ film's interface on sapphire and SiC, respectively, taken with the incident beam parallel to the ($\bar{1}10$) film zone axis. Cross-sectional high resolution TEM shows a sharp interface between β-$Ga_2O_3$ films and $Al_2O_3$ substrate; however, β-$Ga_2O_3$/SiC interface has a metastable $SiO_x$ layer that is polycrystalline in structure as shown in Fig. 5(b). To identify the crystal structure of β-$Ga_2O_3$, SAED and FFT diffraction patterns were indexed (not shown) followed by evaluation of the ratio of the g-vectors as well as the angles between the reflecting planes. From FFT and SAED analysis the

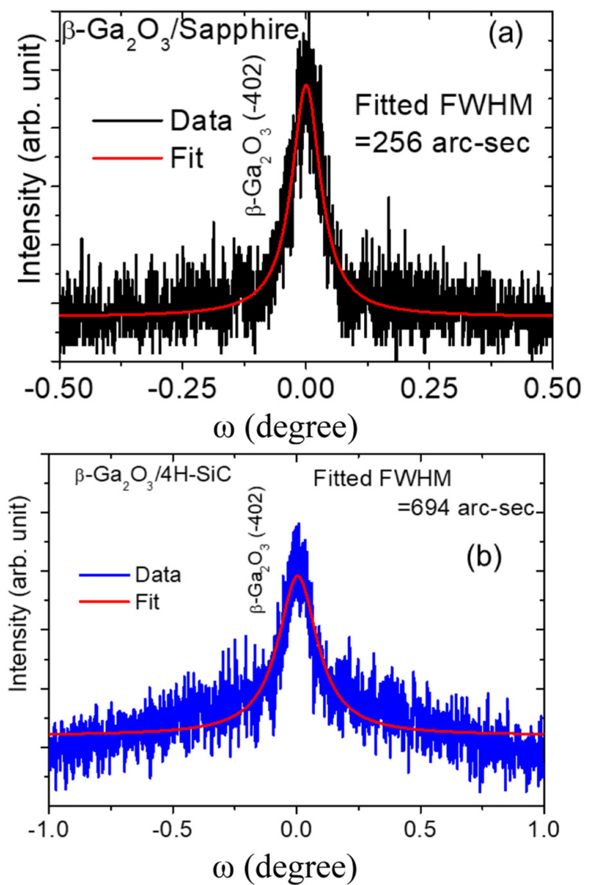


**FIG. 4.** X-ray diffraction rocking curves of β-$Ga_2O_3$ (−402) peak on (a) sapphire and (b) 4H-SiC. Measured RC FWHM are 256 and 694 arc sec, respectively.

measured out-of-plane and in-plane epitaxial relations are ($\bar{2}01$)$Ga_2O_3$//(0001)SiC and $\langle\bar{1}10\rangle$$Ga_2O_3$//$\langle01\bar{1}0\rangle$SiC, respectively. Defect analysis using a composite images of phase contrast and inverse fast Fourier transform lattice images of $Ga_2O_3$/$Al_2O_3$ reveal mostly stacking faults and twinning defects with a density of $2.5 \times 10^{12}$ $cm^{-2}$ and $0.2 \times 10^{12}$ $cm^{-2}$, respectively. Nevertheless, β-$Ga_2O_3$/SiC showed a reduced stacking fault with a density of $\sim 1.0 \times 10^{12}$ $cm^{-2}$; however, twinning was not observed.

The optical properties of the MBE grown β-$Ga_2O_3$ epitaxial layer on sapphire were studied using optical absorption measurement in the range of 200–1200 nm and are shown in Fig. 6. The inset shows a plot of $(\alpha h\nu)^2$ vs hν giving a direct bandgap (Tauc plots-[20]) of 4.90 eV, which is the same as the typically reported bandgap of β-$Ga_2O_3$.[4] Because of the lower bandgap of the 4H-SiC substrate, the β-$Ga_2O_3$/4H-SiC template had strong absorption at 3.2 eV from the bandgap of the SiC substrate (not shown), which prevent bandgap determination of the $Ga_2O_3$ film by this method.

The cathodoluminescence (CL) measurements of β-$Ga_2O_3$ on both sapphire and SiC at room temperature and 5 K are shown in

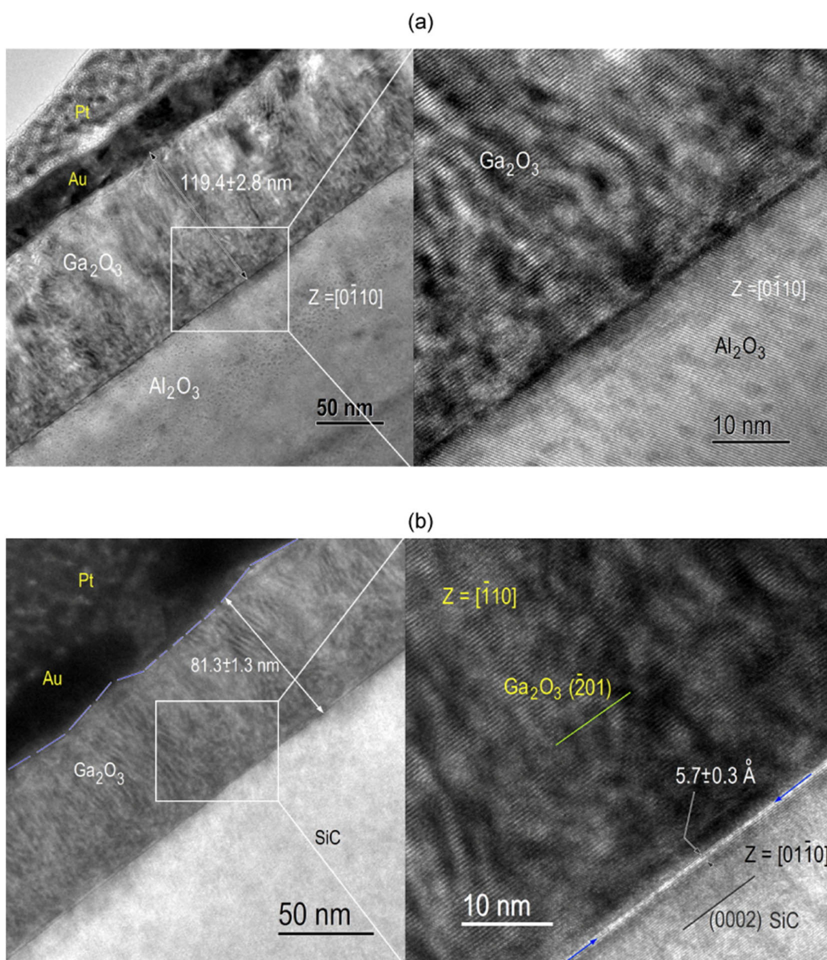


**FIG. 5.** Cross-sectional phase contrast TEM micrographs of (a) β-$Ga_2O_3$ on c-sapphire showing the average film thickness of ∼119.4 ± 2.8 nm and to the right hand side is a high resolution lattice image of the showing perfectly sharp interface and (b) β-$Ga_2O_3$ on SiC with a an average thickness of ∼81.3 ± 1.3 nm, and a thin crystalline interfacial SiOx (∼5.7 ± 0.3 Å) layer.

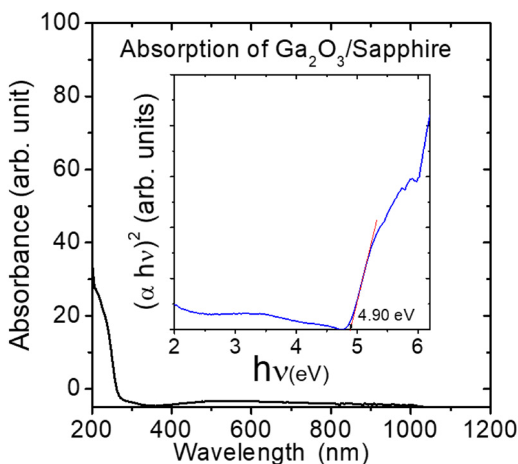


**FIG. 6.** Optical absorption vs wavelength of β-$Ga_2O_3$/sapphire. The insets shows a plot of $(\alpha h\nu)^2$ vs hν giving direct bandgap (Tauc plots).

Figs. 7(a) and 7(b), respectively. 3 keV electrons were used as the excitation source that, as determined by Monte Carlo simulations, has a maximum probe depth by secondary electrons of 80 nm, well within the 84–120 nm thick $Ga_2O_3$ films.[21] In both films, there is no observation of a near band edge peak at around 4.9 eV, which is consistent with previously reported results.[22] Both spectra exhibit a broad emission from the blue to the UV region which could be due to donor-acceptor pair transitions involving oxygen or Ga vacancies and interstitials.[23] The film deposited on the wider-bandgap sapphire substrate shows an intense and dominant broad emission band with peaks around 2.5 eV and 3.0 eV of spectra acquired at room temperature and 3.0 eV at 5 K, respectively. Upon decreasing temperature, the 3.0 eV defect emission band intensity increases compared to that of the 2.5 eV defect emission band intensity. A neutron irradiation study reported that both the 2.5 and the 3.0 eV emission intensities increase with increasing neutron irradiation flux, indicating that both emission bands are likely associated with defects related to gallium vacancies.[23] The intensity of the CL spectra of the film deposited on 4H-SiC is about threefold weaker than that deposited on the sapphire substrate and exhibits a

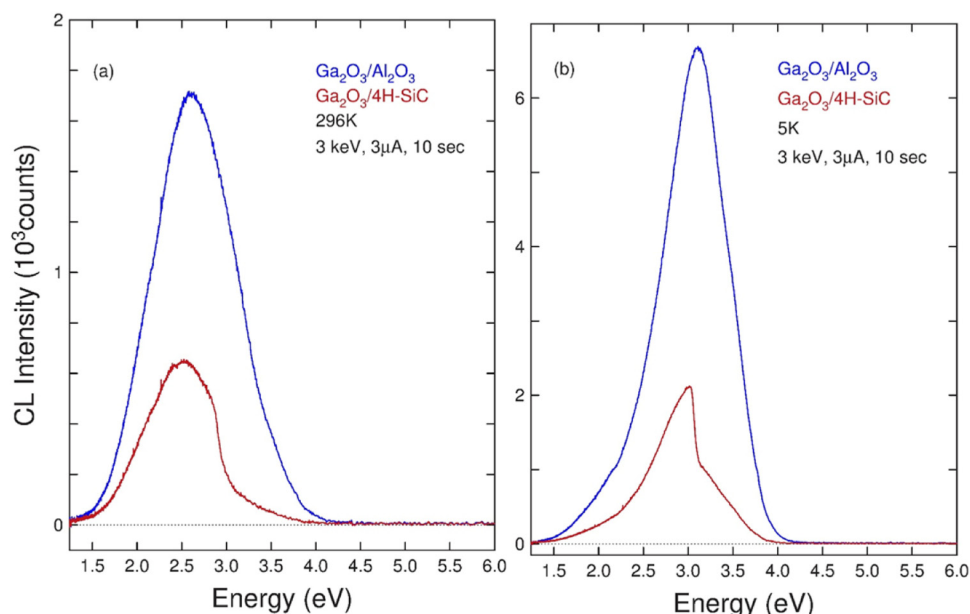


**FIG. 7.** (a) Room temperature and (b) low temperature, 5 K cathodeluminescence spectra of $Ga_2O_3$ films deposited on (a) sapphire and (b) SiC substrates. There is a large CL lineshape variation upon changing temperature.

different spectral intensity distribution. This might be expected because photons emitted at the higher energy side of the β-$Ga_2O_3$ emission band has enough energy to excite the recombination processes in the underlying SiC substrate, which has a smaller bandgap, resulting on the overlapping distribution of CL emission from $Ga_2O_3$ films and photo-excited SiC substrate emission bands. This is consistent with the observed difference on the emission line shapes obtained for films deposited on SiC compared to that on sapphire, which results from the overlap from "pure" $Ga_2O_3$ film emission band and the photo-excited SiC substrate emission bands.

Time-domain thermoreflectance (TDTR)[24,25] was used to measure the thermal conductivity of $Ga_2O_3$ on SiC (not shown). For the estimation of the through-plane thermal conductivity of $Ga_2O_3$, the variation in thermoreflectance of a metallic transducer, expressed as the ratio (R) between the in-phase signal ($V_{in}$) and the out-of-phase signal ($V_{out}$), as a result of the periodic heating of the sample with a laser is compared with a mathematical model.[26,27] The thermal properties are considered parameters that are adjusted iteratively using the Levernberg–Marquardt algorithm, until the differences between the measured data and the model-generated data are minimized. One important consideration is the sensitivity analysis of each parameter. The sensitivity was calculated using Eq. (1),[28]

$$S_p = \frac{\partial \ln\left[-\frac{V_{in}}{V_{out}}\right]}{\partial \ln P} = \frac{\partial \ln R}{\partial \ln P} = \frac{dR/R}{dP/P}, \tag{1}$$

where $P$ represents any of the variables of the mathematical model (e.g., thickness, thermal conductivity, etc.). In practice, this means that the absolute value of the sensitivity for a fitted parameter (thermal conductivity of the thin film, in this case) should be as high as possible. In addition, note that a high sensitivity of one of the nonfitted parameters (thin film layer thickness, for example) indicates that this parameter must be measured accurately. Figure 8 presents a comparison of the sensitivity of the mathematical model to different parameters. Three parameters stand out: the thermal conductivity of $Ga_2O_3$, the specific heat of Al, and the thickness of Al.

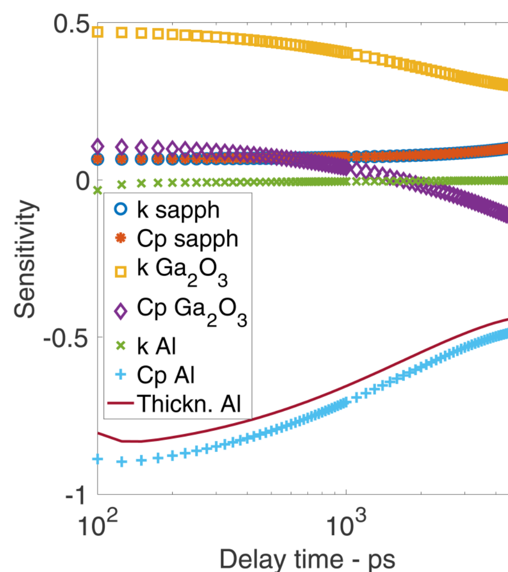


**FIG. 8.** Sensitivity analysis of the $Ga_2O_3$ sample on sapphire, relevant to thermal property measurement using TDTR, for a modulation frequency of 8.8 MHz. In the figure legend, k represents the thermal conductivity and $C_p$ the specific heat.

The high sensitivity of the thermal conductivity of $Ga_2O_3$ indicates that this fitted parameter is accurate. In addition, the uncertainty was calculated following the same procedure explained in Ref. 29. Since the uncertainty depends on the relative sensitivities of the different variables, a high sensitivity translates into a low uncertainty. In summary, the sensitivity analysis of the samples allows us to conclude that the thermal conductivity values presented below are credible.

The through-plane and in-plane thermal conductivities of SiC were estimated to be $301 \pm 36$ W/m K and $387 \pm 46$ W/m K, respectively, using the TDTR technique. In the case of sapphire, an isotropic model was used to obtain a thermal conductivity of $27 \pm 2$ W/m K. These values agree with the literature[30] and were used as parameters to determine the properties of the 3-layered samples. TDTR measured thermal conductivity of the 120 and 81 nm thick $Ga_2O_3$ layer on c-sapphire and 4H-SiC were $3.2 \pm 0.3$ and $3.1 \pm 0.5$ W/m K, respectively. So, thermal conductivity of $Ga_2O_3$ films grown on SiC is measured to be lower than that grown on sapphire. Measured TBC at the $Ga_2O_3$/SiC interface is $142 \pm 64$ MW/$m^2$ K, while at $Ga_2O_3$/sapphire is $156 \pm 65$ MW/$m^2$ K. TBC at the $Ga_2O_3$/SiC interface is similar to $Ga_2O_3$ grown on low conductivity sapphire indicating that $Ga_2O_3$ can be grown on high conductivity SiC without much degradation in interfacial conductance. In addition, the TBC values are sufficiently high such that they will no longer be a limiting value for thin $Ga_2O_3$ films on SiC. The thermal conductivity values of MBE grown $Ga_2O_3$ films are slightly higher than the similar thickness films, reported value of about 2.9 W/m K, grown by pulsed laser deposition on c-sapphire.[31] The thermal conductivity of 100 nm thick poly-crystalline $Ga_2O_3$ films grown via annealing on (0001) GaN surfaces in open atmosphere is measured as 1.88 W/m K by Szwejkowski *et al.*[32] using TDTR. The higher values in our MBE-grown films could confirm that the thermal conductivity depends on the deposition method since the phonons could scatter on deposition-induced crystal defects. In fact, the values determined for the MBE-grown films agree with the theoretical calculations published in Ref. 33, where the thermal conductivity of 100 nm thick $Ga_2O_3$ layers are around 3 W/m K, indicating that the heteroepitaxial thin $Ga_2O_3$ layers fabricated by MBE could produce less defective layers.

## IV. CONCLUSIONS

In summary, RF-plasma MBE was used for the heteroepitaxial growth of ∼100 nm thick β-$Ga_2O_3$ thin films on sapphire and 4H-SiC substrates. Films were extensively characterized using AFM, XRR, optical absorption, XRD, room and low temperature CL, TEM, and TDTR measurements. Room and low temperature CL spectra show $V_{Ga}$ related defects in the film; however, β-$Ga_2O_3$ on SiC is epitaxial. Films on both sapphire and SiC yielded similar morphologies, phase, epitaxy, and thermal properties but different point defect concentrations. MBE β-$Ga_2O_3$ film thermal conductivity is similar or higher than the reported values for the film similarly thick films deposited on sapphire by other methods. TBC for SiC substrate is as good as on low conductivity sapphire, which shows that $Ga_2O_3$ could be fabricated on high conductivity substrate like SiC without much degradation in interface resistance. Further optimization is needed to improve the interface between the substrate and the $Ga_2O_3$ film. Heteroepitaxy of β-$Ga_2O_3$ on high thermal conductivity substrates such as SiC could be one of the approaches to manage its low thermal conductivity in advanced devices. These results demonstrate a pathway to direct integration with higher thermal conductivity substrates that could improve device reliability and performance.

## ACKNOWLEDGEMENTS

This work was supported by the Office of Naval Research (ONR). XRR measurements were conducted at the G2 beamline of the Cornell High Energy Synchrotron Source (*CHESS*).

## REFERENCES


[1] H. Amano *et al.*, J. Phys. D Appl. Phys. **51**, 163001 (2018).
[2] PowerAmerica Roadmap version 1, see https://www.poweramericainstitute.org/wp-content/uploads/2017/01/PowerAmerica_Roadmap_Final-Public-Version-January-2017.pdf, 1-33 (2017).
[3] I. C. Kizilyalli, E. P. Carlson, and D. W. Cunningham, IEEE International Electronic Devices Meeting IEDM-18 (IEEE, New York, 2018), pp. 19.6.1–19.6.4.
[4] J. Y. Tsao *et al.*, Adv. Electron. Mater. **4**, 1600501 (2018).
[5] D. Brunner, H. Angerer, E. Bustarret, F. Freudenberg, R. Höpler, R. Dimitrov, O. Ambacher, and M. Stutzmann, J. Appl. Phys. **82**, 5090 (1997).
[6] F. Yun, M. A. Reshchikov, L. He, T. King, H. Morkoç, S. W. Novak, and L. Wei, J. Appl. Phys. **92**, 4837 (2002).
[7] W. Liu and A. A. Balandin, J. Appl. Phys. **97**, 073710 (2005).
[8] S. J. Pearton, F. Ren, M. Tadjer, and J. Kim, J. Appl. Phys. **124**, 220901 (2018).
[9] H. H. Tippins, Phys. Rev. **140**, A316 (1965).
[10] A. Kuramata, K. Koshi, S. Watanabe, Y. Yamaoka, T. Masui, and S. Yamakoshi, Jpn. J. Appl. Phys. **55**, 1202A2 (2016).
[11] M. D. Santia, N. Tandon, and J. D. Albrecht, Appl. Phys. Lett. **107**, 041907 (2015).
[12] Y. J. Won, J. W. Cho, D. Agonafer, M. Asheghi, and K. E. Goodson, IEEE Trans. Comp. Pack. Man. **5**, 737 (2015).
[13] S. A. O. Russell, A. P. Thomas, C. F. McConville, C. A. Fisher, D. P. Hamilton, P. A. Mawby, and M. R. Jennings, IEEE J. Electron Devices **5**, 256 (2017).
[14] C. Yuan, Y. Zhang, R. Montgomery, S. Kim, J. Shi, A. Mauze, T. Itoh, J. S. Speck, and S. Graham, J. Appl. Phys. **127**, 154502 (2020).
[15] Z. Cheng, L. Yates, J. Shi, M. J. Tadjer, K. D. Hobart, and S. Graham, APL Mater. **7**, 031118 (2019).
[16] Z. Cheng, V. D. Wheeler, T. Bai, J. Shi, M. J. Tadjer, T. Feygelson, K. D. Hobart, M. S. Goorsky, and S. Graham, Appl. Phys. Lett. **116**, 062105 (2020).
[17] S. Nakagomi, K. Yokoyama, and Y. Kokubun, J. Sens. Sens. Syst. **3**, 231 (2014).
[18] S. A. Kukushkin, V. I. Nikolaev, A. V. Osipov, E. V. Osipova, A. I. Pechnikov, and N. A. Feoktistov, Phys. Solid State+ **58**, 1876 (2016).
[19] A. V. Osipov, A. S. Grashchenko, S. A. Kukushkin, V. I. Nikolaev, E. V. Osipova, A. I. Pechnikov, and I. P. Soshnikov, Continuum Mech. Therm. **30**, 1059 (2018).
[20] J. Tauc, Mater. Res. Bull. **3**, 37 (1968).
[21] P. Hovington, D. Drouin, and R. Gauvin, Scanning **19**, 1 (1997).
[22] M. Orita, H. Ohta, and M. Hirano, Appl. Phys. Lett. **77**, 4166 (2000).
[23] H. Gao *et al.*, Appl. Phys. Lett. **112**, 242102 (2018).
[24] T. L. Bougher, L. Yates, C. F. Lo, W. Johnson, S. Graham, and B. A. Cola, Nanosc. Microsc. Therm. **20**, 22 (2016).
[25] D. B. Brown, T. L. Bougher, B. A. Cola, and S. Kumar, Carbon **139**, 913 (2018).
[26] D. G. Cahill, Rev. Sci. Instrum. **75**, 5119 (2004).
[27] J. Liu, J. Zhu, M. Tian, X. Gu, A. Schmidt, and R. Yang, Rev. Sci. Instrum. **84**, 034902 (2013).
[28] R. M. Costescu, M. A. Wall, and D. G. Cahill, Phys. Rev. B **67**, 054302 (2003).

[29]P. Jiang, B. Huang, and Y. K. Koh, Rev. Sci. Instrum. **87**, 075101 (2016).
[30]E. A. Burgemeister, W. V. Muench, and E. Pettenpaul, J. Appl. Phys. **50**, 5790 (1979).
[31]N. Blumenschein, M. Slomski, P. Paskov, F. Kaess, M. H. Breckenridge, J. F. Muth, and T. Paskova, Proc. SPIE **10533**, 105332G (2018).
[32]C. J. Szwejkowski, N. C. Creange, K. Sun, A. Giri, B. F. Donovan, C. Constantin, and P. E. Hopkins, J. Appl. Phys. **117**, 084308 (2015).
[33]D. Q. Tran, N. Blumenschein, A. Mock, P. Sukkaew, H. Zhang, J. F. Muth, T. Paskova, P. P. Paskov, and V. Darakchieva, Phys. B **579**, 411810 (2020).